Journal of Coastal Research	30	4	800–814	Coconut Creek, Florida	July 2014

Colored Dissolved Organic Matter Dynamics in the Northern Gulf of Mexico from Ocean Color and Numerical Model Results

Nazanin Chaichitehrani[†], Eurico J. D'Sa[†]*, Dong S. Ko[‡], Nan D. Walker[†], Christopher L. Osburn[§], and Robert F. Chen[††]

[†]Department of Oceanography and Coastal Sciences
Louisiana State University
Baton Rouge, LA 70803, U.S.A.

[‡]Naval Research Laboratory
Stennis Space Center, MS 39529, U.S.A.

[††]Environmental, Earth, and Ocean Sciences
University of Massachusetts, Boston
Boston, MA 02125, U.S.A.

[§]Department of Marine, Earth and Atmospheric Science
North Carolina State University
Raleigh, NC 27695, U.S.A.

www.cerf-jcr.org

www.JCRonline.org

ABSTRACT

Chaichitehrani, N.; D'Sa, E.J.; Ko, D.S.; Walker, N.D.; Osburn, C.L., and Chen, R.F., 2014. Colored dissolved organic matter dynamics in the Northern Gulf of Mexico from ocean color and numerical model results. *Journal of Coastal Research,* 30(4), 800–814. Coconut Creek (Florida), ISSN 0749-0208.

Colored dissolved organic matter (CDOM) absorption and salinity relationships were assessed and used in conjunction with the salinity and current outputs of a numerical model (Navy Coastal Ocean Model [NCOM]) to study CDOM dynamics in the northern Gulf of Mexico. *In situ* CDOM absorption and salinity obtained from multiple field campaigns were inversely correlated seasonally (winter–spring and summer) and latitudinally (inner- and outer-shelf zones), suggesting conservative behavior of CDOM distribution. A weaker correlation, during summer in the outer-shelf zone, however, indicated stronger effects of photooxidation and lower masking effects from riverine CDOM. Applying these relationships to simulated salinity resulted in hourly maps of CDOM that revealed similarities to CDOM patterns derived from *SeaWiFS* satellite imagery. Further, matchup comparisons between model-derived and *in situ* CDOM absorption were statistically sound for the summer (bias = –0.016, root mean square error = 0.059, $r^2 = 0.51$ SI = 0.28) and the winter–spring periods (bias = 0.033, root mean square error = 0.099, $r^2 = 0.52$, SI = 0.21). Overlaying the model-derived CDOM maps on the simulated currents revealed the strong influence of currents on CDOM advection. Downcoast currents during the nonsummer months led to persistent advection of CDOM westward interrupted by frequent cold front events that flush CDOM-laden waters out of the coastal bays onto the inner and outer continental shelves. In contrast, the upcoast current regime, though less well organized, produces a more significant seaward advection of CDOM, likely due to the Ekman transport and subsequent entrainment by mesoscale eddies over the continental slope.

ADDITIONAL INDEX WORDS: *CDOM, salinity, SeaWiFS, NCOM model.*

INTRODUCTION

Chromophoric dissolved organic matter (CDOM) in natural waters absorbs light in the ultraviolet (UV) and visible wavelength range and plays a key role in regulating light attenuation in the aquatic medium. In coastal waters, CDOM is predominantly a mixture of terrestrial sources (*e.g.*, humic and fulvic acids) that is introduced to coastal systems by river runoff. By contrast, CDOM in the open ocean is predominantly a mixture of autochthonous sources, such as phytoplankton and its subsequent heterotrophic processing (Blough and Del Vecchio, 2002; Nelson *et al.*, 2007, and references therein). There is increasing interest in monitoring CDOM due to its numerous influences and applications. Its light-absorbing properties can significantly impact primary productivity by limiting light while also blocking harmful UV radiation (Stedmon *et al.*, 2000). CDOM has been used as an intermediary for determination of dissolved organic carbon concentrations using remote sensing (Del Castillo and Miller, 2008; Griffin *et al.*, 2011). In coastal waters, CDOM has been employed as a semiconservative water mass tracer, as an indicator of water mass mixing, and as an index to measure water quality (Blough and Del Vecchio, 2002; Coble *et al.*, 2004; D'Sa and Korobkin, 2008; Ferrari and Dowell, 1998; Le Fouest *et al.*, 2006). Further, CDOM can also be used as a proxy for retrieving salinity using ocean color sensors and providing synoptic maps of salinity (Bowers and Brett, 2008; D'Sa *et al.*, 2002). Since CDOM plays an important role in various biogeochemical cycles and microbial ecology in natural waters (Moran and Zepp, 1997), it is critical to study its distribution and fate in the aquatic environment. Although satellite ocean color data have been used to retrieve and monitor CDOM (D'Sa, Miller, and Del Castillo, 2006; Kahru and Mitchell, 2001; Mannino, Russ, and Hooker, 2008), their more regular use in monitoring and applications is hampered by cloud coverage and sun glint effects. Cloud coverage often limits acquisition of clear imagery, while sun glint can confound precise retrieval of water's constituents from remote sensors (Yoder, 1999). Further, use of satellite data is limited by the satellite's temporal and spatial resolution and the time of the satellite

DOI: 10.2112/JCOASTRES-D-13-00036.1 received 14 February 2013; accepted in revision 9 August 2013; corrected proofs received 25 October 2013; published pre-print online 18 December 2013.
*Corresponding author: ejdsa@lsu.edu

pass. In contrast, numerical circulation model outputs such as temperature and salinity that can be directly or indirectly derived from satellite data can be generated at much higher temporal and spatial resolution. Hence, it would be desirable to find an approach to extract CDOM from the outputs of a numerical model. The strong linkage between salinity and CDOM reported in many studies especially in coastal waters suggests that salinity could be used as a proxy to derive CDOM from simulated salinity. However, in order to use numerical models to derive an ocean color product such as CDOM there is a requirement for (1) a strong inverse linear relationship between CDOM and salinity and (2) a reliable numerical model to simulate salinity.

The relationship between absorption coefficients of CDOM (a_{CDOM}) and salinity has been studied for different regions (D'Sa *et al*., 2002; Ferrari and Dowell, 1998; Stedmon and Markager, 2003). In coastal regions highly influenced by CDOM-laden river runoff, a_{CDOM} often declines linearly with increasing salinity, indicating that CDOM behaves conservatively with respect to salinity, suggesting a simple dilution process with neither addition nor removal of terrestrial CDOM (Blough and Del Vecchio, 2002; Blough, Zafiriou, and Bonilla, 1993; Ferrari and Dowell, 1998; Kowalczuk, 1999; Vodacek *et al*., 1997). Nonlinear relationships between a_{CDOM} and salinity have been reported in different aquatic environments, including coastal regions (Blough, Zafiriou, and Bonilla, 1993; Chen and Gardner, 2004; Gardner, Chen, and Berry, 2005; Kowalczuk, 1999). An upward or a downward deviation from an inverse linear relationship between CDOM and salinity suggests an addition (*e.g*., autochthonous production) or removal (*e.g*., photodegradation, adsorption) of CDOM (D'Sa and DiMarco, 2009; Uher *et al*., 2001) or the mixing of multiple water masses with different CDOM end members (Chen and Gardner, 2004; Ferrari and Dowell, 1998; Stedmon and Markager, 2003; Uher *et al*., 2001). In such cases, caution should be taken in using salinity as a proxy for CDOM.

Currents and salinity outputs of numerical models such as the Navy Coastal Ocean Model (NCOM) can be used in conjunction with CDOM derived using CDOM–salinity relationships to investigate physical influences on CDOM distributions. Advection of CDOM by currents is an important physical process that could affect CDOM distribution in the northern Gulf of Mexico. Jolliff *et al*. (2003) combined a circulation model with CDOM photolysis to study CDOM transport over the west Florida shelf (WFS). Their circulation model included advection–dispersion equations of pollutant transport with modified source terms to include CDOM transport. Following model verification with *in situ* measurements and satellite data, simulation results were employed to study CDOM distribution patterns over the WFS. Shulman *et al*. (2011) combined the remotely sensed parameters and the outputs of the NCOM model to study the effects of the California current system on optical parameters. In the northern Gulf of Mexico, better insights on the spatial and temporal distribution and fate of CDOM could be obtained by understanding the current patterns and use of model simulations.

Various factors such as winds, river discharges, and detached eddies from the Loop Current can contribute to the generation of currents over the Louisiana–Texas shelf (Li, Nowlin, and Reid, 1997; Oey, 1995; Walker, 2005; Walker *et al*., 1996, 2005). Results from a modeling study indicate that a large component of transport over the inner shelf is produced by wind (40–48%), with river discharge (28–33%) and Loop Current (LC) eddies (19–33%) accounting for the rest (Oey, 1995). Two seasonal current patterns that depend on wind characteristics are distinguishable over the shelf (Cho, Reid, and Nowlin, 1998; Cochrane and Kelly, 1986; Walker, 2005). During nonsummer months (from September to May), the large-scale circulation on the Louisiana–Texas continental shelf exhibits a cyclonic gyre, driven mainly by easterly winds, Ekman transport, and geopotential (Cochrane and Kelly, 1986). A strong coastal jet forms the northern limb of this gyre, which is modulated by discharge from the Mississippi and Atchafalaya Rivers (Cho, Reid, and Nowlin, 1998; Cochrane and Kelly, 1986; Walker, 2005) in addition to winds. Jarosz and Murray (2005) aptly named it the Louisiana–Texas Coastal Current (LTCC). This inner shelf current, also known as a downcoast current, is well developed with a clear westward direction from Louisiana to Texas and southward along the Texas coast (Cho, Reid, and Nowlin, 1998; Walker, 2005; Wiseman and Kelly, 1994). The frequent passage of cold fronts in nonsummer months subjects the LTCC to strong W and NW winds for one to several days duration (Walker, 2005). The wind reversals have a rapid impact on surface circulation and often on the strength and duration of the LTCC (Murray *et al*., 1998; Walker, 2005; Walker and Hammack, 2000).

Eastward-directed outer shelf currents form the outer limb of the cyclonic gyre (Cochrane and Kelly, 1986) and the presence of LC anticyclonic eddies often enhance the eastward flow on the outer shelf even though their centers are in waters ~1000 m deep (Cho, Reid, and Nowlin, 1998; Walker, 2005; Walker *et al*., 1996). The downcoast current weakens and disappears during summer months (June, July, and August) (Cochrane and Kelly, 1986; Walker, 2005) as a result of a wind shift from E to S and SW. This change in the wind direction starts along the south Texas inner shelf usually in May, initiating an upcoast current that strengthens and expands to the Louisiana shelf as summer progresses (Cochrane and Kelly, 1986; Jarosz, 1997; Walker, 2005). The upcoast current is not as well developed as the downcoast current and exhibits a disorganized pattern (Allahdadi, Jose, and Patin, 2012; Crout, Wiseman, and Chuang, 1984; Jarosz and Murray, 2005). During summer, shelf-break currents are still directed to the east, and no gyre is formed. The downcoast current is reestablished by September when easterly winds resume (Cochrane and Kelly, 1986; Walker, 2005), and it persists for much of the time from then until sometime in May (Cochrane and Kelly, 1986; Walker, 2005). These synoptic and seasonal patterns of wind behavior, as well as the seasonality of river discharges (Li, Nowlin, and Reid, 1997), are likely to contribute strongly to the formation of distinct patterns of CDOM distribution over the shelf.

Therefore, the main objective of the present study is to examine physical influences on surface CDOM distribution

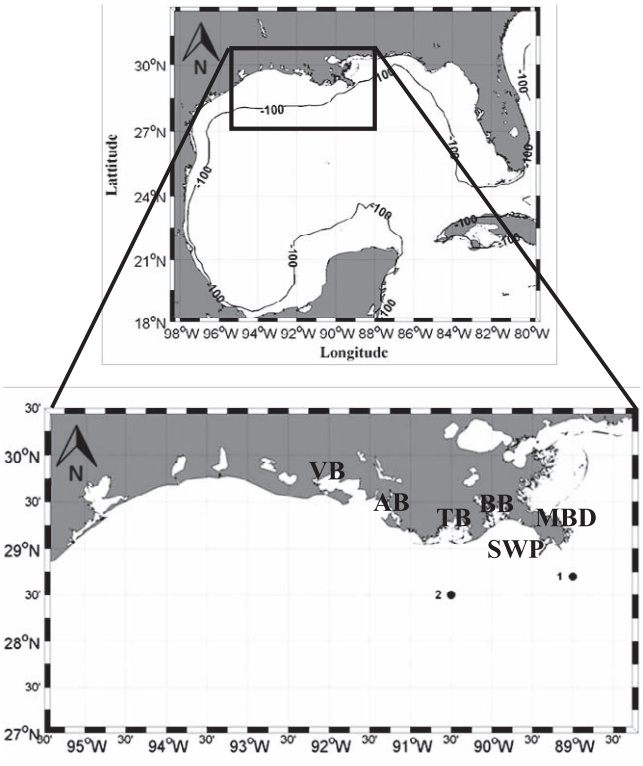

Figure 1. Map of the study region in the northern Gulf of Mexico encompassing Mississippi, Louisiana, and parts of Texas coast. Black circles show the locations for which MsLaTex simulated current velocities were acquired for March and June 2005. MBD = Mississippi Birdfoot Delta, SWP = Southwest Pass, BB = Barataria Bay, TB = Terrebonne Bay, AB = Atchafalaya Bay, VB = Vermillion Bay.

using NCOM numerical model outputs of salinity and currents. The study includes two parts; the first part assesses the relationship between CDOM absorption and salinity using a large database of *in situ* measurements over the study area to derive CDOM from simulated salinity. CDOM–salinity relationships were determined for different zones and seasons, which were then applied to the simulated salinity maps. The second part investigates the role of advective influences using simulated current patterns on CDOM distribution under three main physical regimes of downcoast, upcoast, and cold front passages in the northern Gulf of Mexico.

DATA AND METHODS

Study Area

The Northern Gulf of Mexico, comprising both the inner and outer shelf areas between 88.2°W to 95.5°W and latitude 27°N to 30.5°N, were studied using field and satellite ocean color data along with the outputs from a numerical model (Figure 1).

The inner-shelf region of this area is characterized by high amounts of discharge from the Mississippi and Atchafalaya Rivers, which is characterized by distinct seasonality with peak flow in spring and low flow in autumn (Müller-Karger *et al.*, 1991; Walker *et al.*, 1994). This large volume discharge of freshwater strongly affects the physical and biogeochemical processes over the study area (D'Sa and Miller, 2003; Lohrenz, Dagg, and Whitledge, 1990; Müller-Karger *et al.*, 1991; Walker and Rabalais, 2006). Although the river discharge increases CDOM and decreases salinity in the coastal waters, they can both be modulated by shelf hydrodynamics.

Field Data

CDOM and salinity data were obtained from nine oceanographic cruises carried out in 2001 (April), 2005 (March, May, July, and August), 2006 (January), 2007 (April and May), and 2009 (August) (Table 1). The sampling locations are shown for the winter–spring (Figure 2A) and the summer (Figure 2B) periods. In 2005 (March, May, July, and August), water samples were obtained from the nearshore coastal waters strongly influenced by the Mississippi and Atchafalaya Rivers (west of Southwest Pass, off the Terrebonne Bay, and Atchafalaya shelf) aboard the R/V *Gyre* (D'Sa and DiMarco, 2009).

Water salinity was measured using a conductivity–temperature–depth profiler (Sea-Bird Electronic, Inc., Bellevue, Washington, U.S.A.) during all cruises. Water samples on the R/V *Gyre* cruises were filtered through prerinsed 0.2-μm Nucleopore membrane filters. Filtered samples were kept refrigerated at 4°C, and absorption coefficients were measured on single-beam or dual-beam spectrophotometers. Optical absorbance spectra measured from 250 to 722 nm using Milli-Q water as a reference were further corrected for baseline fluctuations by subtracting the average absorbance between 715 and 722 nm (D'Sa and DiMarco, 2009). The absorption coefficients (m^{-1}) for each wavelength were then obtained using the expression

$$a(\lambda) = \frac{2.303A(\lambda)}{l} \quad (1)$$

where A is the absorbance, λ is the wavelength, and l is the optical path length in meters (0.1 m or 0.5 m). Similar methods for field sampling and data analysis were used to obtain CDOM and salinity data for samples acquired from other field campaigns. More detailed information can be found in the Biological and Chemical Oceanography Data Management Office Web site (http://data.bco-dmo.org/jg/serv/BCO/NACP_Coastal/GulfMexico/CDOM.html).

Satellite Data

Data from the *SeaWiFS* ocean color sensor (August 1997 to December 2010) were used to derive CDOM absorption coefficients at 412 nm ($a_{cdom}(412)$). Daily *SeaWiFS* Level-1 merged local area coverage data with 1-km resolution were obtained from the Ocean Color Web site run by the National Aeronautics and Space Administration (NASA) (oceancolor.gsfc.nasa.gov) and processed using *SeaWiFS* Data Analysis System (SeaDAS) into Level-2 to obtain CDOM absorption by applying the (D'Sa *et al.*, 2006) empirical algorithm given by the equation:

$$a_{CDOM}(412) = 0.227[R(510)/R(555)]^{-2.512} \quad (2)$$

where $R_{rs}(510)$ and $R_{rs}(555)$ are remote sensing reflectances at 510 and 555 nm wavelength bands, respectively. The robust-

Table 1. *Summary of cruises undertaken in the northern Gulf of Mexico showing periods when samples were acquired for this study. Average values for $a_{CDOM}(412)$ and salinity shown for each cruise.*

Cruise	Date	$a_{CDOM}(412)$ (m^{-1})	Salinity (psu)
1	12–16 April 2001	0.23	30.20
2	23–29 March 2005	0.47	27.07
3	20–25 May 2005	0.43	25.96
4	8–12 July 2005	0.23	29.27
5	18–24 August 2005	0.25	28.75
6	1–4 January 2006	0.43	23.50
7	7–10 May 2007	0.87	24.16
8	16–20 April 2007	0.41	31.75
9	18–20 August 2009	0.34	27.94

ness of this algorithm was demonstrated based on matchup comparisons with field data (Chaichitehrani *et al*., 2012, unpublished data). The *SeaWiFS*-derived surface CDOM absorption images were used to compare with NCOM-derived CDOM maps.

NCOM Data

A high spatial resolution (~1.9 km) nested Navy Coastal Ocean Model (NCOM) previously developed for the Mississippi–Louisiana–Texas (MsLaTex) coast as part of a NASA-funded project was used in this study (D'Sa and Ko, 2008). The NCOM MsLaTex coastal model covers the region between 27°N and 30.5°N latitude and between 88.2°W and 95.5°W longitude (372 × 200 grid) and includes the Mississippi, Louisiana, and Texas shelves and the offshore waters in the northern Gulf of Mexico (Figure 1). The MsLaTex model is nested within the Intra-Americas Sea Nowcast/Forecast System (IASNFS) and is based on the NCOM (Barron *et al*., 2006; Martin, 2000), a primitive equation model with hybrid sigma-z vertical coordinates. The model horizontal resolution is between 1.8 and 1.9 km, which resolves well the major circulation features on the shelf. The model topography is derived from NRL 2-min global topography data set (DBDB2) and improved with hydrographic data from National Geophysical Data Center. There are 111 rivers or freshwater runoff points included in the model with daily river discharges from the Army Corps of Engineers and U.S. Geological Survey stations to better simulate the coastal salinity. The surface forcing of wind, heat, and air pressure are from the Coupled Ocean/Atmosphere Mesoscale Prediction System high-resolution regional weather forecast model. The boundary conditions for the MsLaTex model were imported from the IASNFS. IASNFS includes the Gulf of Mexico, the Caribbean, and parts of the western North Atlantic with horizontal resolution of ~6 km. Both IASNFS and MsLaTex models assimilate sea surface height anomaly data from satellite altimeters (*GFO*, *Jason-1*, and *ERS-2*) and sea surface temperature data from the Advanced Very High Resolution Radiometer to reproduce the important mesoscale Loop Current and Loop Current Eddies in the Gulf of Mexico (D'Sa and Ko, 2008; Ko *et al*., 2008).

RESULTS

CDOM–Salinity Relationship

Conservative behavior between CDOM absorption and salinity is essential to employ salinity as a proxy for the determination of CDOM. For the study area, the inverse linear relationship between CDOM absorption and salinity was found to vary seasonally and spatially; seasonal variability in discharges from the Mississippi and Atchafalaya Rivers, enhanced water column mixing during the winter–spring season, and elevated CDOM photobleaching and stratification during summer likely contributed to this variability. Field data collected during various cruises (Table 1) were examined, and CDOM–salinity relationships were established for the winter–spring and summer periods spatially partitioned into two latitudinal zones (Figures 2A and B; Table 2). Zone 1 comprises the shallow areas east of the Birdfoot Delta and the inner shelf west of the delta. Zone 2 comprises the deeper outer shelf extending from Mississippi to the east Texas shelf. Zone 1 is directly affected by the discharge from the Mississippi and Atchafalaya Rivers. In zone 1, effects due to photobleaching are most likely masked by the lower salinity waters containing elevated levels of CDOM (D'Sa and DiMarco, 2009). In contrast, zone 2 is less affected by the rivers' freshwater, and therefore less conservative behavior of CDOM and salinity is expected. This is generally in accordance with the shelf division suggested by Nowlin *et al*. (2005) in connection with studies of the long-term flow along the Texas–Louisiana shelf.

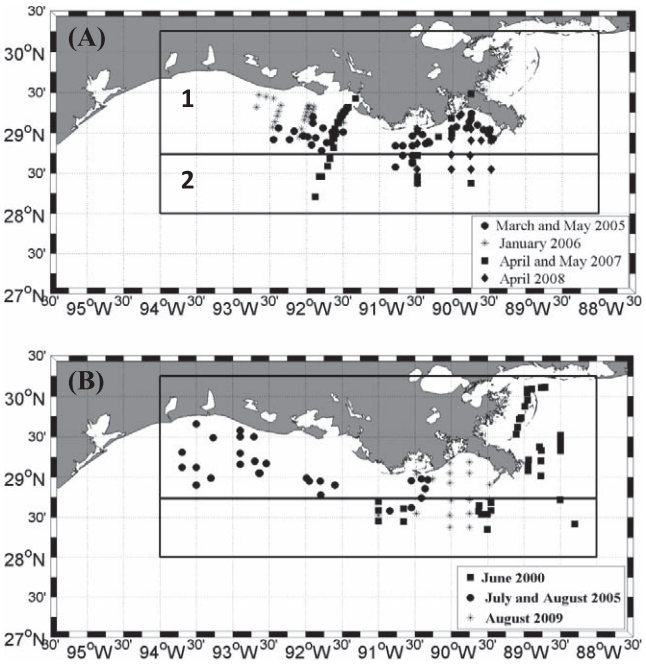

Figure 2. Station locations of cruises conducted during (A) winter–spring, and (B) summer periods. Zones 1 and 2 are indicated.

The surface CDOM absorption coefficient at 412 nm was 0.61 ± 0.57 m^{-1} at an average surface salinity of 26.06 ± 8.22 during winter–spring in zone 1, indicating the strong river influence on CDOM and salinity fields in the nearshore waters. During the same period, zone 2 exhibited an average surface salinity of 32.66 ± 4.47, and an average CDOM absorption of

Table 2. *Geographical extension of zone 1 and zone 2.*

Subset Region	Latitude Range	Longitude Range
Zone 1	28.73°N–30.25°N	88.00°W–94.00°W
Zone 2	28.00°N–28.729°N	88.00°W–94.00°W

0.203 ± 0.18 m^{-1}, which was three times less than that of the zone 1. During summer, surface CDOM in zone 1 (0.32 ± 0.22 m^{-1}) was almost two times less than the winter–spring period, while the mean surface salinity over this zone increased slightly to 27.47 ± 3.62. Lower CDOM in zone 1 during the summer could be attributed to the low flow of the Mississippi and the Atchafalaya Rivers and to photobleaching effects aided by stratification and high solar insolation (Boss *et al.*, 2001; D'Sa and DiMarco, 2009). Zone 2 during summer exhibited the lowest CDOM absorption (0.064 ± 0.103 m^{-1}) and highest salinity (32.84 ± 2.72), suggesting loss of CDOM due to photochemical decomposition (Chen and Gardner, 2004; Opsahl and Benner, 1998).

For each season and each zone, the CDOM absorption coefficient at 412 nm, $a_{\mathrm{CDOM}}(412)$, were plotted as a function of salinity (Figures 3A–D; Table 3). High correlations between CDOM and salinity were obtained for both the winter–spring and summer periods in zone 1 ($r^2 = 0.88$, $n = 117$; $r^2 = 0.92$, $n = 39$, respectively) (Figure 3A–C) suggesting conservative mixing between coastal and oceanic waters in support of results of D'Sa and DiMarco (2009). Similarly, for zone 2, CDOM and salinity were highly correlated during the winter–spring period ($r^2 = 0.93$, $n = 22$) (Figure 3B), likely as a result of mixing associated with frontal passages during the period. In contrast, during summer, $a_{\mathrm{CDOM}}(412)$ exhibited low correlations with salinity (Figure 3D), and many of the data points fell below a conservative mixing line, which could be attributed to photooxidation and loss of CDOM during the summer.

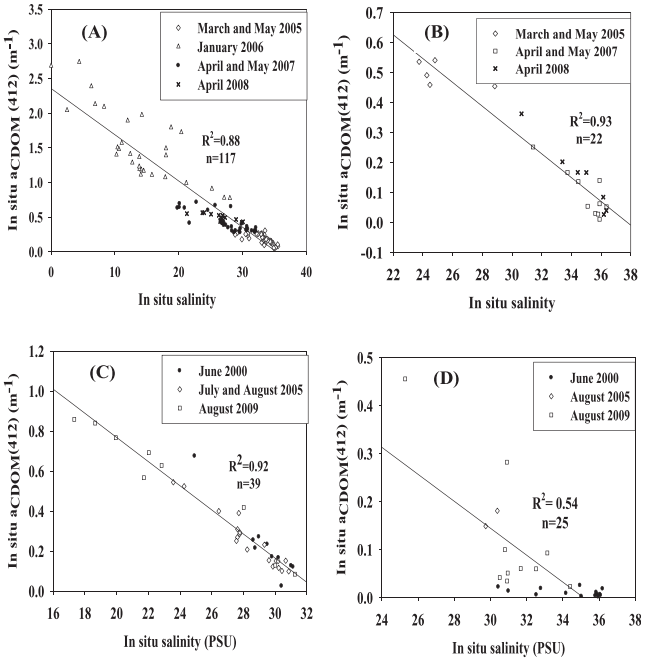

Figure 3. Correlations between $a_{\mathrm{CDOM}}(412)$ and salinity (A) for the winter–spring period in zone 1, (B) for the winter–spring period in zone 2, (C) for summer in zone 1, (D) for the summer in zone 2.

Table 3. *Results showing the slope (***a***), intercept (***b***) and correlation coefficient (r^2) of the regression equation*[a] *between* $\mathbf{a}_{CDOM}(412)$ *and salinity for the two zones.*

Subset Region	Season	Number of Samples	*a*	*b*	r^2
Zone 1	Winter–spring	117	−0.066	2.35	0.88
Zone 2	Winter–spring	22	−0.039	1.49	0.93
Zone 1	Summer	39	−0.060	1.98	0.92
Zone 2	Summer	25	−0.028	0.98	0.54

[a] An inverse (negative) linear relationship was fitted between $a_{\mathrm{CDOM}}(412)$ (m^{-1}) and salinity in the form of $a_{\mathrm{CDOM}}(412) = a \times \text{salinity} + b$, where a is the slope and b is the intercept.

Spatial Distribution of CDOM Based on Modeled Salinity

The accuracy of NCOM MsLaTex model for simulating salinity was examined by comparing modeled and *in situ* salinity for available salinity data (Figure 4). Error statistics such as bias, root mean square error (RMSE), scatter index (SI), and correlation coefficient (r^2) were calculated using the following equations:

$$\mathrm{Bias} = \frac{1}{N}\sum_{i=1}^{N}(y_i - x_i) \tag{3}$$

$$\mathrm{RMSE} = \sqrt{\frac{1}{N}\sum_{i=1}^{N}(y_i - x_i)^2} \tag{4}$$

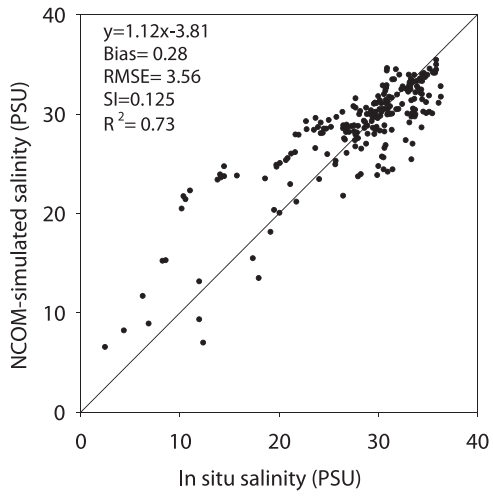

Figure 4. Comparison of *in situ* salinity with simulated salinity. The diagonal line is the 1-to-1 line.

$$\mathrm{SI} = \frac{1}{\bar{x}}\sqrt{\frac{1}{N}\sum_{i=1}^{N}[(y_i - \bar{y}) - (x_i - \bar{x})]^2} \quad (5)$$

where y_i denotes simulated values, x_i denotes field measured values, $\bar{y}$ is the average of simulated value, and $\bar{x}$ is the average of *in situ* values. N is number of samples. Error statistics (bias = 0.28, RMSE = 3.56, SI = 0.12, and $r^2 = 0.73$ for $n = 225$) indicated relatively satisfactory performance of the model in simulating salinity.

CDOM–salinity relationships (Table 3) were applied to modeled salinity to obtain model-derived CDOM absorption maps (*e.g.*, Figures 5A and B). These were compared with *SeaWiFS*-derived CDOM absorption imagery obtained using the D'Sa, Miller, and Del Castillo (2006) algorithm. Based on availability of clear satellite imagery for the study area, modeled outputs for 18 October 2005 and 23 July 2005 (1900 h UT) were selected as representatives for nonsummer and summer periods, respectively. Figures 5A–C and 6A–C show simulated salinity maps, model-derived CDOM maps, and *SeaWiFS*-derived CDOM absorption for both the selected times. The simulated salinity on 18 October 2005 (Figure 5A) shows that the entire study area except some regions adjacent to the mouths of the Mississippi and Atchafalaya Rivers were influenced by high salinity values (~35 psu on average). The low-salinity regions were limited to areas around the Mississippi Birdfoot Delta, Southwest Pass, Barataria, Terrebonne, Atchafalaya, and Vermilion Bays. This was not unexpected, since river discharges are normally at their lowest in autumn.

The inverse and linear relationships between CDOM and salinity determined for the study area implies that high CDOM is expected in the low-salinity coastal region and low CDOM in the high-salinity offshore waters. This is illustrated in a map of surface CDOM absorption derived from simulated salinity (Figure 5B). A comparison of the model-derived surface CDOM and *SeaWiFS*-derived CDOM for 18 October 2005 at 1830 hours UT (Figure 5C) shows similar patterns of CDOM distributions. Entrainment of CDOM from the Southwest Pass of the Mississippi River toward the inner shelf in the simulated map appeared similar to the *SeaWiFS*-derived image, as was the pattern at the mouth of the Atchafalaya Bay.

Simulated salinity was selected for 23 July 2005 at 1900 hours UT as representative of summer along with *SeaWiFS* imagery for the same day (Figure 6). The simulated salinity (Figure 6A) depicts low-salinity filaments extending outward from the South Pass of the Mississippi River delta. This pattern appears as high-surface CDOM in the vicinity of South Pass extending toward the shelf break until it disperses and mixes with high-salinity offshore waters. Model simulation also shows the CDOM-laden low-salinity waters spreading east of the Birdfoot Delta toward the continental shelf of the NE Gulf of Mexico (Figure 6B). Although the derived CDOM exhibits high consistency with the satellite image (Figure 6C), especially for coastal areas, overestimates in satellite-derived CDOM in the very nearshore waters, especially west of the Atchafalaya Bay system, could be due to interference from seawater constituents such as suspended sediments and algal biomass (D'Sa, 2008).

The ability of the model to simulate CDOM was investigated by comparing the MsLaTex model-derived CDOM with *in situ* measurements for the winter–spring and the summer periods (Figures 7A and B, respectively). Model data used for matchup comparisons were acquired from simulations for May, March, July, and August 2005 concurrent with *in situ* data and were independent of the data used for the investigation of CDOM conservative behavior. Results show that the model-derived CDOM was quantitatively in agreement with the field data. For the winter–spring, average measured and modeled $a_{\mathrm{CDOM}}(412)$ was 0.44 m^{-1} and 0.48 m^{-1} (bias = 0.03; RMSE = 0.099; SI = 0.21, and $r^2 = 0.52$), while for the summer, the average values of $a_{\mathrm{CDOM}}(412)$ were 0.2 m^{-1} and 0.18 m^{-1} (bias = –0.016, RMSE = 0.059, SI = 0.28, and $r^2 = 0.51$), respectively. These results demonstrate the MsLaTex model's ability to predict patterns of surface CDOM in the study area. In addition, the match-up comparison between *SeaWiFS*-derived CDOM using the D'Sa, Miller, and Del Castillo (2006) algorithm and *in situ* measurements for the winter–spring and the summer periods was shown by Tehrani *et al.* (2013).

Effect of Advection on CDOM Distribution

Advection by currents is the main physical process that affects the distribution of CDOM after being discharged into the marine environment by rivers (here the Mississippi and the Atchafalaya Rivers) (Boss *et al.*, 2001). Seasonal or weather-related reversals in the direction of currents on the shelf along with the seasonal variations in rivers' discharge and CDOM levels can lead to significant spatial and temporal variabilities in surface CDOM distribution. In order to study CDOM distribution in relation to horizontal advection, surface CDOM derived from modeled salinity was superposed over the simulated current. This revealed that the CDOM distribution patterns corresponded to cold front passage events and expected patterns for the seasonal downcoast and upcoast current regimes during 2005. These maps suggest strong physical influences on CDOM distribution and are examined further for each of the above cases.

Figure 8 depicts hind-cast CDOM distributions overlaid with modeled surface currents for 5 May 2005 (1800 h UT) that show a representative downcoast current regime, except that the offshore limb of the cyclonic gyre is weak to nonexistent. The general current direction over the inner shelf is westward, with an average current velocity of 0.5 m/s. Approaching the shelf break, current velocity increases to approximately 1 m/s. A large anticyclonic Loop Current Eddy offshore of the Mississippi Birdfoot Delta induced strong eastward currents at the shelf break. In general, the persistent direction of shelf currents to the west entrained CDOM from coastal areas toward the inner and midshelf regions. Current characteristics during May were further studied by examining time series NCOM currents at points 1 and 2 (Figures 9A and D) located south of the Mississippi Birdfoot Delta and off the Terrebonne Bay, respectively (see Figure 1 for location). At point 1, W and SW currents were dominant for the first 5 days of May (Figure 9A), while SE to NE currents were prevalent for the rest of the month. Point 2 exhibited longer periods of downcoast current patterns with intermittent southward changes in current direction induced by cold front passage events. CDOM-rich

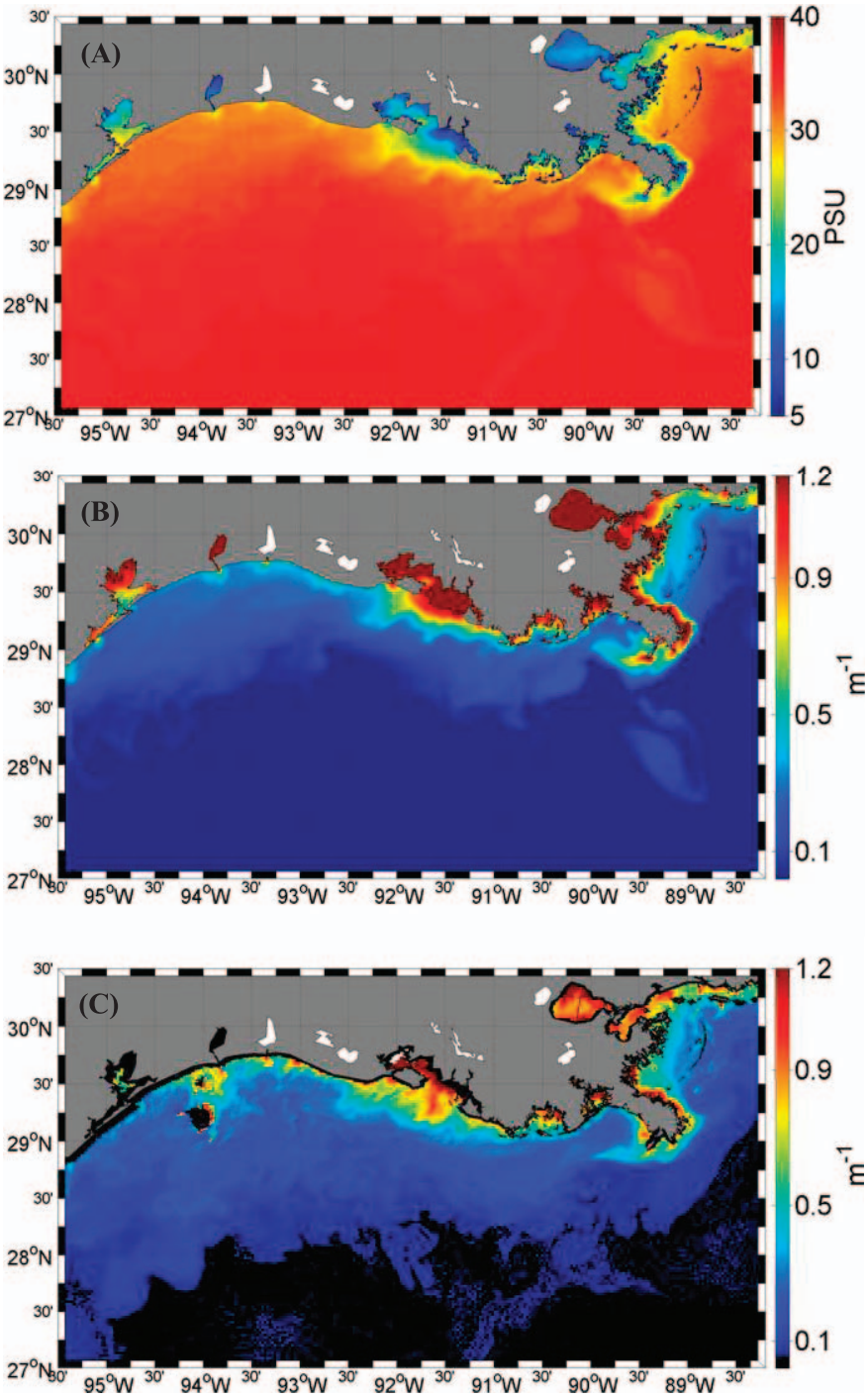

Figure 5. (A) MsLaTex simulated salinity map, (B) model-derived CDOM absorption map for 18 October 2005, at 1900 h UT, and (C) *SeaWiFS*-derived CDOM absorption map for 18 October 2005, at 1830:24 h UT. (Color for this figure is available in the online version of this paper.)

waters ($a_{CDOM}(412)$ 1.2 m^{-1} or more) west of the Mississippi Birdfoot Delta and off the Atchafalaya Bay were advected by westward shelf currents downcoast. The high surface CDOM south of the Birdfoot Delta was not entrained toward the outer shelf, since the current pattern implies an east to west CDOM advection. CDOM absorption was relatively high (0.8–1 m^{-1}) in the Louisiana Bight or the region between Southwest Pass of the Mississippi Birdfoot Delta and Barataria Bay. The modeled current patterns indicate that CDOM-laden waters were trapped in this region as a result of an anticyclonic (clockwise)

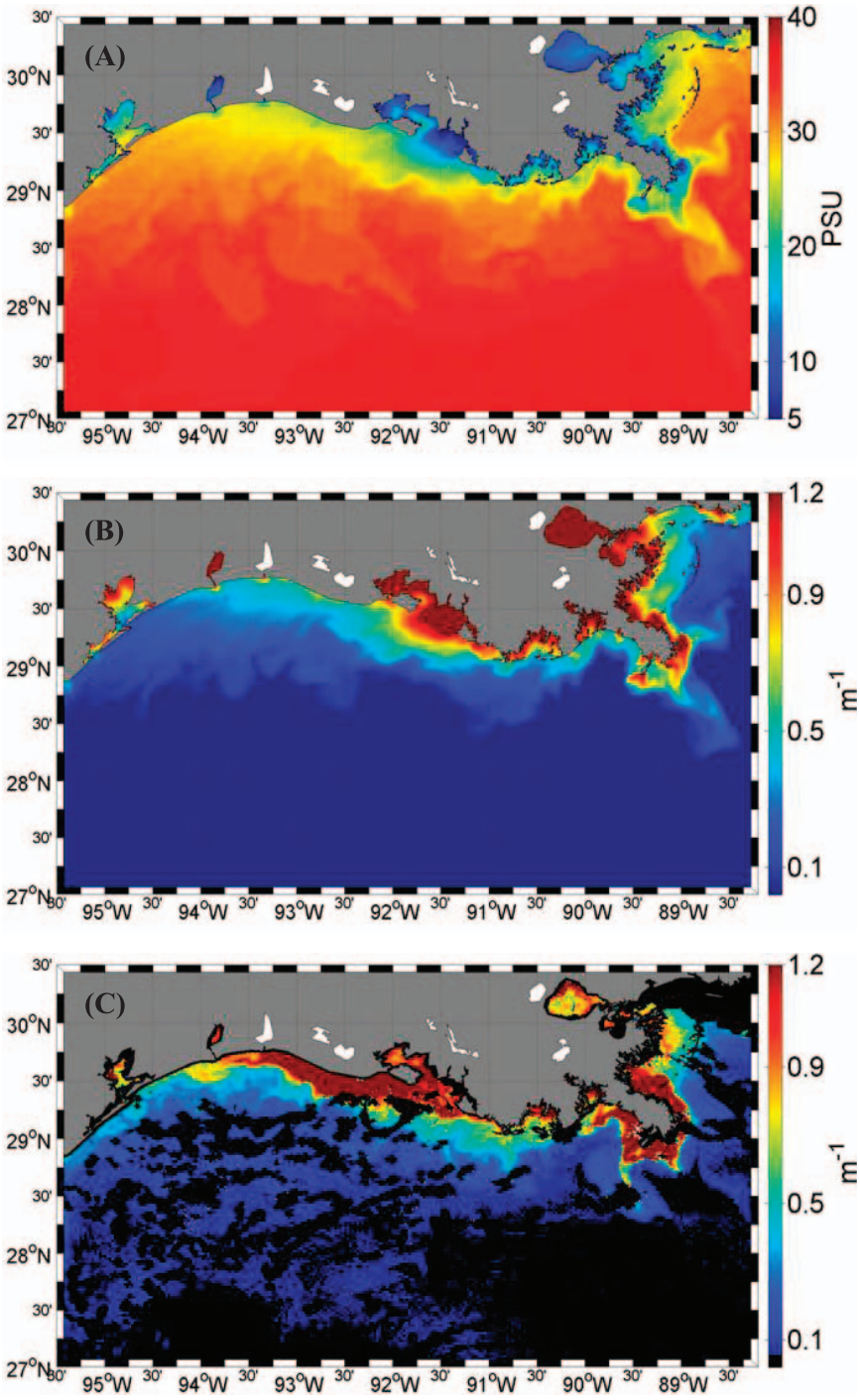

Figure 6. (A) MsLaTex simulated salinity map, (B) model-derived CDOM absorption map for 23 July 2005, at 1900 h UT, and (C) *SeaWiFS*-derived CDOM map for 23 July 2005, at 1851:23 h UT. (Color for this figure is available in the online version of this paper.)

gyre generated by the rotation of the Mississippi River plume that originated off Southwest Pass and other passes to the east (Figure 10).

Figure 11 illustrates the model-derived CDOM pattern overlaid with modeled currents on 11 March 2005 at 1200 hours UT, associated with a cold front passage event. Frequent cold fronts disturbed the westward downcoast current system during March (Figures 9C and E). For example, this event was associated with NW winds that induced S to SE currents with a velocity of 0.2 to 0.8 m/s on the inner Louisiana–Texas shelf. On

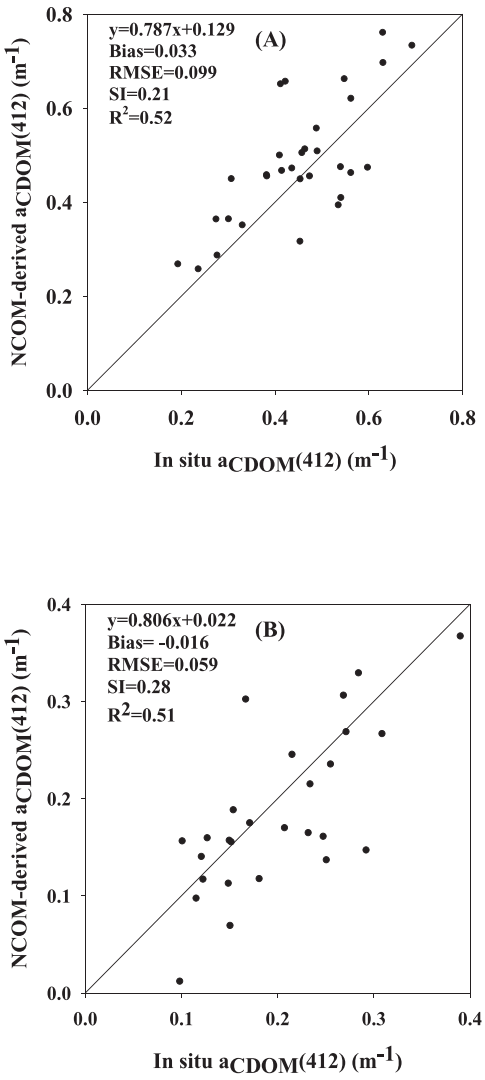

Figure 7. Match-up comparison between model-derived CDOM absorption and *in situ* CDOM (A) for the winter–spring period, and (B) for the summer.

the outer shelf, the currents were eastward, most likely due to the impact of large mesoscale eddies. Time series of currents for both point 1 (Figure 9B) and point 2 (Figure 9E) during this period showed significant southward currents as a result of cold front outbreaks. The current reached a maximum velocity of 0.8 and 0.6 m/s at points 1 and 2, respectively. The corresponding CDOM pattern was strongly tied to the current pattern. The general southward direction of currents on the inner shelf advected CDOM-laden waters toward the outer shelf. CDOM-rich waters (CDOM absorption of 1.2 m^{-1} and greater) from the Atchafalaya–Vermillion and Terrebonne–Timbalier Bays were flushed out and injected onto the inner shelf during the cold front passage event. The same process also advected CDOM offshore from Texas estuaries and coastal areas onto the eastern Texas shelf.

Typical surface currents influencing CDOM distribution for the summer (22 June 2005, at 0000 h UT) are illustrated in Figure 12. Shelf currents were relatively disorganized with a general eastward direction, which is consistent with an upcoast current regime. Shelf-break currents to the S and SW of the Birdfoot Delta were eastward and influenced by a mesoscale anticyclonic eddy located offshore of the Mississippi Canyon at latitude 27°30′N. The average inner-shelf current velocity at this time was ~0.3 m/s. Vector representation of currents at point 1 (Figure 9C) during June showed a general upcoast pattern with current velocity up to 0.8 m/s. There was a general eastward current direction for the first 9 days of June, but later strong SW currents with velocities up to 1.5 m/s affected the shelf area for 2 days. The direction of S currents changed to NE as a result of the upcoast current regime on 22 June. As observed, the current pattern at point 1 was complex and could be attributed to factors such as wind forcing, Loop Current eddies, and the influence of the Mississippi River plume (Martínez-López and Zavala-Hidalgo, 2009; Nowlin *et al.*, 2005; Walker *et al.*, 2005). Point 2 (Figure 9F) experienced low current velocities during the first 10 days of June (less than 0.2 m/s); within the next 7 days strong NW to NE currents (maximum velocity of 1 m/s), likely induced by a mesoscale eddy, were dominant at this location. The current velocities decreased by 20 June and by the end of June increased and were directed southward with velocity of 0.5 m/s under the influence of a mesoscale eddy located offshore of the Mississippi Canyon at the latitude of 27°30′N. On the eastern Texas shelf, elevated CDOM was widely distributed over the shelf, presumably as a result of Ekman transport induced by W and SW winds. An increase in current velocity (up to 0.6 m/s) off the Atchafalaya Bay advected CDOM-laden waters toward the Louisiana shelf, while an increase in current velocity south of Barataria Bay entrained CDOM southward.

DISCUSSION

CDOM and Salinity Behavior

CDOM can be used as a passive proxy to track freshwater masses and salinity (Binding and Bowers, 2003; D'Sa and Miller, 2003; D'Sa *et al.*, 2002; Ferrari and Dowell, 1998). The negative linear relationship, detected for waters within our study region, between salinity and CDOM demonstrates a reasonably conservative behavior of these two parameters modulated by seasonality of river discharge. The dependency of CDOM on salinity was demonstrated for two different zones during the winter–spring and the summer periods. CDOM and salinity were highly correlated in zone 1 for the winter–spring and summer periods, suggesting CDOM distribution was regulated by mixing (Chen *et al.*, 2007). Elevated levels of CDOM associated with low-salinity waters in zone 1 indicate allochthonous sources of CDOM (Toming *et al.*, 2009). In addition, high concentration of CDOM introduced by the Mississippi and the Atchafalaya River runoff to the inner shelf can mask variations induced by removal and addition processes such as photobleaching and microbial activities, respectively (Chen *et al.*, 2004; D'Sa and DiMarco, 2009). In fact, Walker *et al.* (2005) suggested that as much as 75% of the Mississippi River discharge may be advected to the shelf region west of the

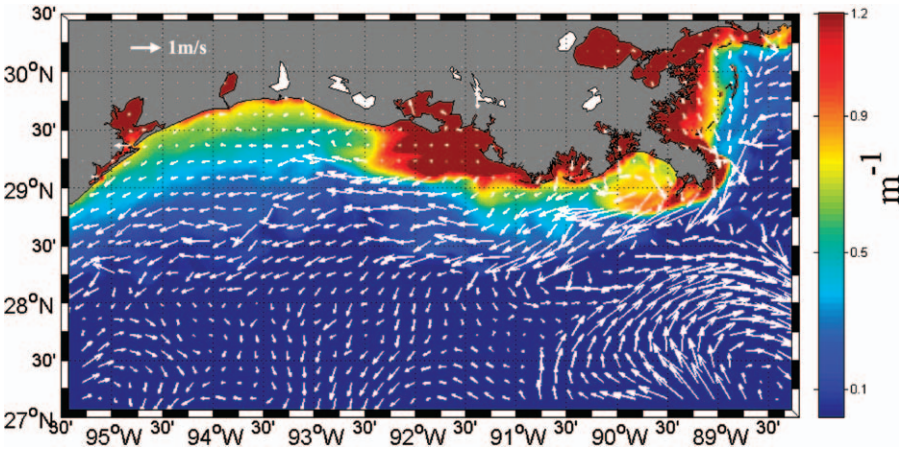

Figure 8. Simulated current pattern for 5 May 2005, at 1800 h UT (color bar indicates CDOM absorption coefficient at 412 nm (m^{-1})). (Color for this figure is available in the online version of this paper.)

Mississippi Birdfoot Delta. This indicates that the Terrebonne Bay area is highly affected by CDOM-rich water from the Mississippi River. Solar illumination and water column stratification during the summer causes photochemical decomposition of CDOM, which disturbs the inverse linear relationship between CDOM and salinity. However, the CDOM–salinity relationship for zone 1 in summer exhibited a strong inverse linear relationship (*i.e.* conservative behavior). This could be attributed to the masking effect of the Mississippi and the Atchafalaya discharge (D'Sa and DiMarco, 2009). Furthermore, the required time scale for CDOM photoxidation is days to weeks, which is longer than the time needed for river-laden CDOM to affect the inner shelf and coastal areas (Hitchcock *et al.*, 2004; Vodacek *et al.*, 1997).

A different seasonal behavior in terms of the CDOM–salinity relationship was observed in zone 2. A strong conservative behavior of CDOM and salinity during the winter–spring period ($r^2 = 0.93$) was observed. In contrast, the summer time relationship suggested a poor conservative behavior of CDOM ($r^2 = 0.54$), which indicated the removal of CDOM, presumably by photodegradation. The footprint of CDOM photodegradation can be identified in Figure 3D by data points that were scattered below the linear CDOM–salinity relationship. The strength of photobleaching over this offshore zone in the summer was accentuated by the low river discharge and absence of its masking impact, which is less prominent over zone 2 during the summer time. Dilution of river CDOM increases the relative depth of photodegradation, enhancing CDOM's removal in surface waters (Osburn, Retamal, and Vincent, 2009). In addition, an increase in salinity over zone 2 may increase CDOM's photoreactivity, especially at longer wavelengths used for remote sensing (Osburn and Morris, 2003; Osburn, O'Sullivan, and Boyd, 2009).

The conservative relationships between CDOM and salinity obtained using a seasonal and zonal approach generally resulted in higher accuracy CDOM concentration maps from simulated salinity. The similarity between CDOM's distribu-

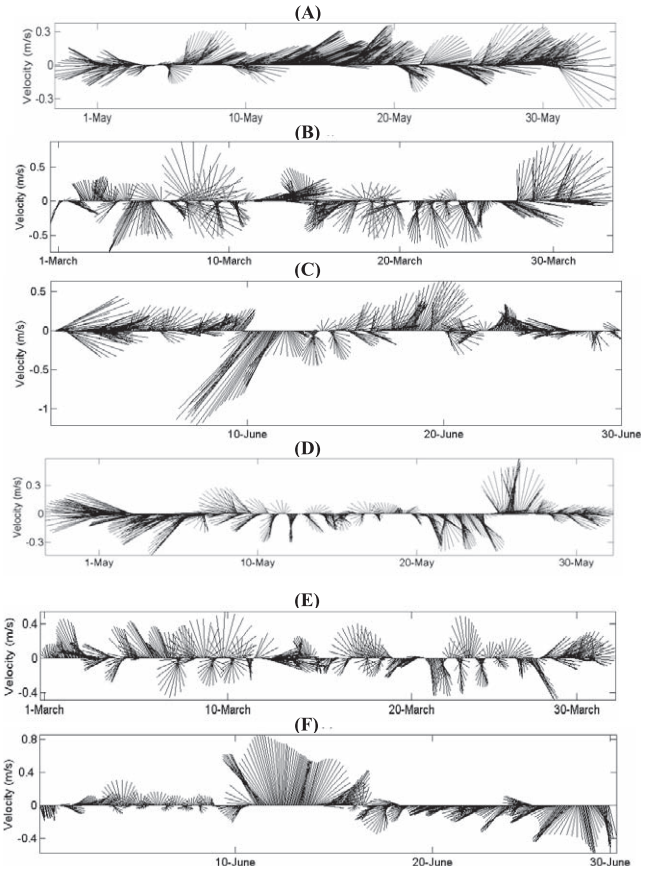

Figure 9. Time series of current (A) at point 1 for May 2005, (B) at point 1 for March 2005, (C) at point 1 for June 2005, (D) at point 2 for May 2005, (E) at point 2 for March 2005, and (F) at point 2 for June 2005 (see Figure 1 for points 1 and 2 locations).

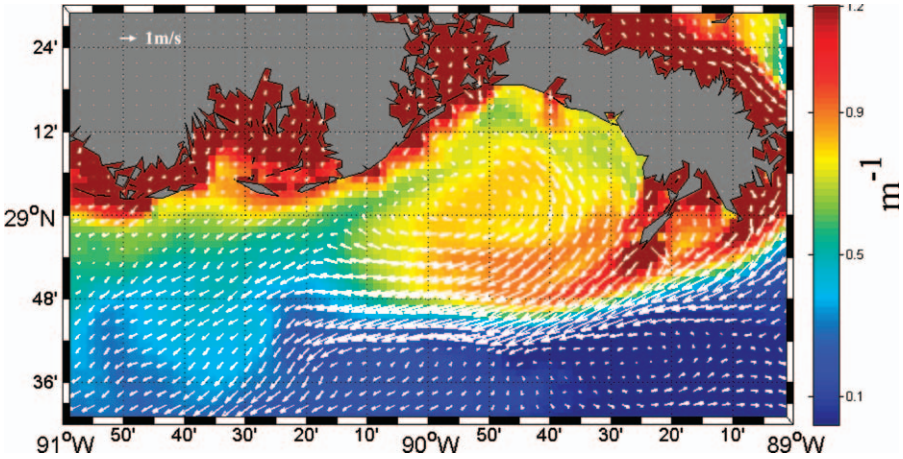

Figure 10. Anticylonic gyre pattern in the Lousiana Bight on 5 May 2005 (1800 h UT) (color bar indicates CDOM absorption coefficient at 412 nm (m^{-1})). (Color for this figure is available in the online version of this paper.)

tion maps obtained from model and *SeaWiFS* data suggests that the approach for producing CDOM synoptic maps using simulated salinity and CDOM–salinity conservation concepts is an appropriate method. However, discrepancies between model-derived and *SeaWiFS*-derived surface CDOM are observed in estuaries and very shallow waters. These could be due to errors in atmospheric correction and interference by the other optically active seawater constituents (D'Sa, 2008; Le Fouest *et al.*, 2006; Walker and Rabalais, 2006). Model deficiency in simulating salinity in coastal areas may also contribute to a lower accuracy of CDOM estimation in these regions. Model-derived CDOM maps can be used as supplemental data to fill temporal and spatial gaps in the satellite data.

Advection and CDOM Distribution

The role of horizontal advection on CDOM distribution on the inner and outer shelves was demonstrated during different current regimes. Cold front passages induce southward currents and strongly contribute to the CDOM advection over the Louisiana shelf. The current can flush CDOM-laden water out of the bays toward the shelf. Walker and Hammack (2000) estimated that 30–50% of the Atchafalaya Bay system's volume is flushed onto the inner shelf during cold front passages. Feng (2009) reported that strong cold fronts could flush more than 40% of the bay waters to the shelf within a period of less than 40 hours, indicating these events are responsible for major outward flushing from the bays. The significant effect of N and NW winds on the flushing of water out of the bays has also been demonstrated using satellite data and numerical models (Cobb, Keen, and Walker, 2008; Walker and Hammack, 2000). Thus, relatively high southward current velocities over the shelf associated with the cold fronts also advect CDOM. Figure 13B illustrates CDOM distribution superposed with isobaths

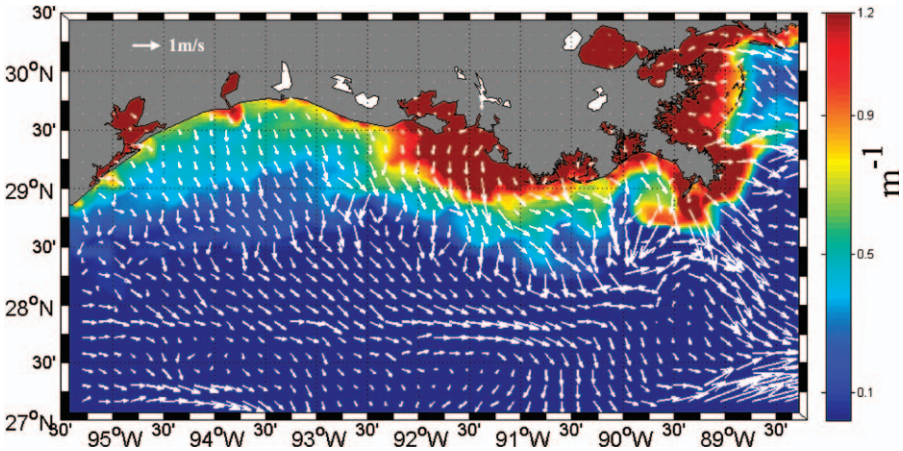

Figure 11. Current pattern for 11 March 2005 at 1200 h UT (color bar indicates CDOM absorption coefficient at 412 nm (m^{-1})). (Color for this figure is available in the online version of this paper.)

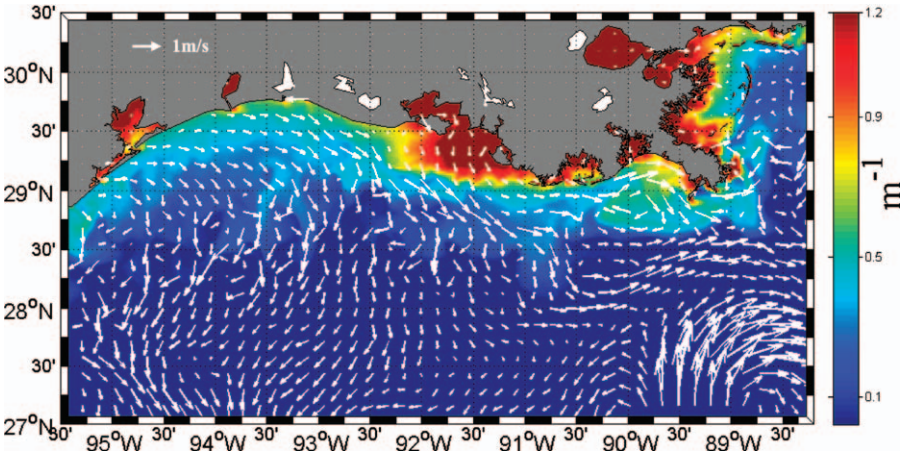

Figure 12. Current pattern for 22 June 2005, at 0000 h UT superposed on CDOM (color bar indicates CDOM absorption coefficient at 412 nm (m^{-1})). (Color for this figure is available in the online version of this paper.)

over the inner and outer shelves for 11 March 2005. Owing to the influence of the wind and southward advection caused by the cold front, elevated CDOM was detected seaward to the 60-m isobath off the Terrebonne Bay, to the 30-m isobath off the Atchafalaya Bay, and to the 40-m isobath off the eastern Texas coast. Westward-directed downcoast currents contributed less to advection of CDOM toward the outer shelf compared with the cold front–induced currents. While cold front–induced currents advected CDOM to ~50-m isobath (on average), downcoast current regimes transport CDOM to ~30-m isobath (Figures 13A and B).

The persistent westward/downcoast current regime may lead to the formation of a relatively high CDOM zone parallel to the Louisiana and eastern Texas coast due to freshwater discharge from rivers. In the Louisiana Bight, a clockwise quasi-permanent easterly wind-driven gyre traps freshwater discharge from the Mississippi River and results in an increase in stratification (Walker and Rabalais, 2006) and relatively high CDOM levels.

Significant increases in buoyancy and stratification over the inner shelf due to advection of the Mississippi River discharge have been reported by Wiseman *et al.* (1997). Although the upcoast current regime is not as organized as that of the downcoast current, CDOM can be advected farther offshore during upcoast currents. As shown in Figure 13C, CDOM is entrained seaward to the 60-m isobath off the Terrebonne Bay, the 50-m isobath off the Atchafalaya Bay, and the 50-m isobath off the eastern Texas coast. This distribution could be due to Ekman transport induced by W and SW winds, which are prevalent during the upcoast current regime. In addition, mesoscale eddies can influence currents on the outer shelf, contributing to offshore entrainment of CDOM. Further, during summer, the general pattern is upcoast currents transporting salty water from the western Gulf of Mexico and Texas to the Louisiana shelf (Li, Nowlin, and Reid, 1997). This advection of salty water may also disturb the conservative relationship between CDOM and salinity in summer.

SUMMARY AND CONCLUSION

The combined use of a numerical model and remote sensing data provides a valuable tool to investigate CDOM dynamics with high spatial and temporal resolution in the northern Gulf of Mexico. Accordingly, an approach was developed to construct synoptic maps of surface CDOM absorption for the region using modeled salinity. The main requirement for implementing this approach was converting salinity to CDOM. This can be successfully accomplished when CDOM covaries inversely with salinity. Field data of CDOM and salinity from different field campaigns were used to examine the seasonal and spatial dependence of CDOM on salinity. The conservative behavior was met for both the inner- and outer-shelf zones during the winter–spring period, while the summer conservative behavior could only be met over the inner-shelf zone due to the masking influence of rivers' runoff on the destructive effects of photodegradation. The resulting CDOM–salinity relationships were applied to simulated salinity to produce CDOM maps for different physical regimes over the study area. The NCOM-derived surface CDOM distribution maps were compared with *SeaWiFS*-derived CDOM absorption maps (D'Sa, Miller, and Del Castillo, 2006), and a satisfactory agreement was observed. Also, the remarkable agreement between *in situ* and NCOM-derived $a_{CDOM}(412)$ as shown by a quantitative evaluation reveals the model's ability to predict CDOM with hourly temporal resolution. Some disparities that were seen between these two maps, especially in estuaries and shallow water regions, could be attributed to the model's drawback in simulating salinity in these regions. Satellite CDOM estimates contaminated by other optically active seawater constituents could also induce further discrepancies. Simulated currents were further applied to investigate CDOM advection over the study area by overlaying simulated currents over the model-

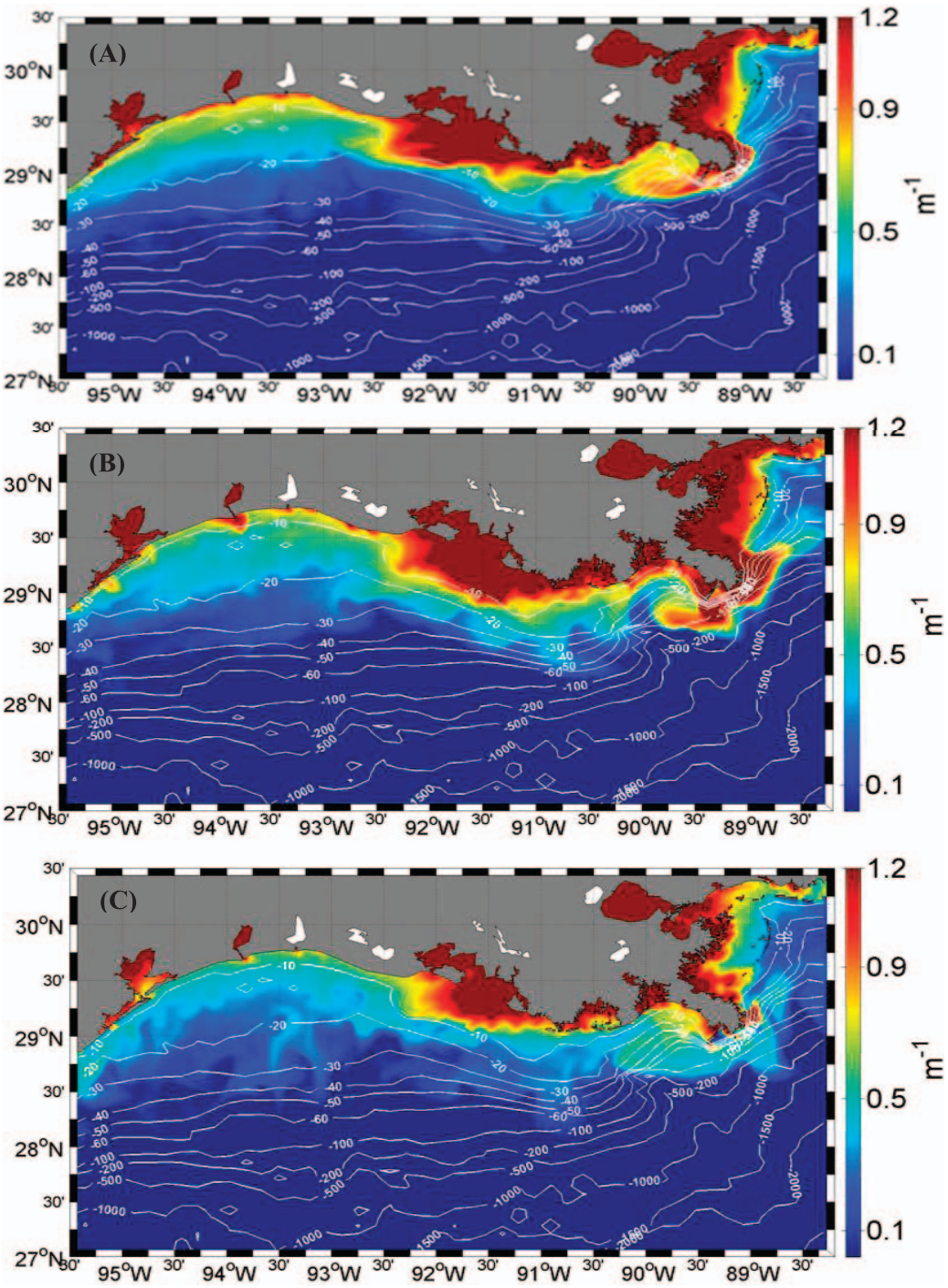

Figure 13. Surface CDOM absorption map derived from model (A) on 5 May 2005 at 1800 hours UT (B) on 11 March 2005 at 1200 h UT and (C) on 22 June 2005 at 0000 h UT. (Color for this figure is available in the online version of this paper.)

derived CDOM maps. The impact of advection on CDOM distribution was demonstrated through a detailed comparison for the upcoast and the downcoast current regimes with the corresponding model-derived CDOM patterns. Southward currents induced by cold front passage events advect CDOM-laden waters from coastal bays to the inner and outer shelf, while the persistent westward downcoast current regime contributed less to CDOM advection toward the outer shelf. The downcoast current regime produces continuous CDOM advection within the LTCC along the Louisiana and eastern

Texas coastlines. Seaward CDOM advection into deep water during an upcoast current regime can be significant due to Ekman transport and the influence of mesoscale eddies on outer shelf currents.

This study demonstrates the suitability of the approach to generate high-resolution CDOM maps based on simulated salinity. Since the base of this approach is the conservative behavior of CDOM and salinity, it is possible to reverse it. Hence salinity can be obtained using satellite data. This would be desired when salinity data are not available or reliable. However, the study area is a highly complex and dynamic environment, and uncertainties associated with microbial and photochemical removal mechanisms and biological sources of CDOM need to be incorporated in future studies.

ACKNOWLEDGEMENTS

The authors acknowledge support provided by a NASA grant NNX09AR7OG that enabled data access through the Biological and Chemical Oceanography Data Management Office (BCO-DMO) website. This work has also been partially supported by a NASA grant NNA07CN12A (Applied Sciences Program) and by a Bureau of Ocean Energy Management Cooperative Agreement 1435-0104CA32806 to E. D'Sa.

LITERATURE CITED

Allahdadi, M.N.; Jose, F., and Patin, C., 2012. Seasonal hydrodynamics along the Louisiana Coast: implications for hypoxia spreading. *Journal of Coastal Research,* 29(5), 1092–1100.

Barron, C.N.; Kara, A.B.; Martin, P.J.; Rhodes, R.C., and Smedstad, L.F., 2006. Formulation, implementation and examination of vertical coordinate choices in the Global Navy Coastal Ocean Model (NCOM). *Ocean Modelling*, 11, 347–375.

Binding, C.E. and Bowers, D.G., 2003. Measuring the salinity of the Clyde Sea from remotely sensed ocean colour. *Estuarine Coastal and Shelf Science*, 57(4), 605–611.

Blough, N.V. and Del Vecchio, R., 2002. Chromophoric DOM in the coastal environment. *In:* Hansell, D.A. and Carslon, C.A. (eds.), *Biogeochemistry of Marine Dissolved Organic Matter*. San Diego, California: Academic, pp. 509–578.

Blough, N.V.; Zafiriou, O.C., and Bonilla, J., 1993. Optical absorption spectra of waters from the Orinoco River outflow—terrestrial input of colored organic matter to the Caribbean. *Journal of Geophysical Research*, 98(C2), 2271–2278.

Boss, E.; Pegau, W.S.; Zaneveld, J.R.V., and Barnard, A.H., 2001. Spatial and temporal variability of absorption by dissolved material at a continental shelf. *Journal of Geophysical Research*, 106(C5), 9499–9507.

Bowers, D.G. and Brett, H.L., 2008. The relationship between CDOM and salinity in estuaries: an analytical and graphical solution. *Journal of Marine Systems*, 73(1–2), 1–7.

Chen, R.F.; Bissett, P.; Coble, P.; Conmy, R.; Gardner, G.B.; Moran, M.A.; Wang, X.C.; Wells, M.L.; Whelan, P., and Zepp, R.G., 2004. Chromophoric dissolved organic matter (CDOM) source characterization in the Louisiana Bight. *Marine Chemistry*, 89(1–4), 257–272.

Chen, R.F. and Gardner, G.B., 2004. High-resolution measurements of chromophoric dissolved organic matter in the Mississippi and Atchafalaya River plume regions. *Marine Chemistry*, 89, 103–125.

Chen, Z.; Hu, C.; Comny, R.N.; Müller-Karger, F., and Swarzenski, P., 2007. Colored dissolved organic matter in Tampa Bay, Florida. *Marine Chemistry*, 104, 98–109.

Cho, K.; Reid, R., and Nowlin, W.D., 1998. Objectively mapped stream function fields on the Texas-Louisiana shelf based on 32 months of moored current meter data, *Journal of Geophysical Research*, 103(C5), 10,377–10,390.

Cobb, M., Keen, T.R., and Walker, N.D., 2008. Modeling the circulation of the Atchafalaya Bay system. Part 2: river plume dynamics during cold fronts. *Journal of Coastal Research*, 24, 1048–1062.

Coble, P.G.; Hu, C.; Gould Jr., R.W.; Chang, G., and A.M. Wood., 2004. Colored dissolved organic matter in the coastal ocean. *Oceanography*, 17, 50–59.

Cochrane, J.D. and Kelly, F.J., 1986. Low-frequency circulation on the Texas-Louisiana continental shelf. *Journal of Geophysical Research*, 91(C1), 10645–10659.

Crout, R.L.; Wiseman, W.J., and Chuang, W.S., 1984. Variability of wind-driven currents, west Louisiana inner continental-shelf: 1978–1979. *Contributions in Marine Science*, 27, 1–11.

Del Castillo, C.E. and Miller, R.L., 2008. On the use of ocean color remote sensing to measure the transport of dissolved organic carbon by the Mississippi River plume. *Remote Sensing of Environment*, 112(3), 836–844.

D'Sa, E.J., 2008. Colored dissolved organic matter in coastal waters influenced by the Atchafalaya River, USA: effects of an algal bloom. *Journal of Applied Remote Sensing*, 2(1), 023502.

D'Sa, E.J. and DiMarco, S.F., 2009. Seasonal variability and controls on chromophoric dissolved organic matter in a large river-dominated coastal margin. *Limnology and Oceanography*, 54(6), 2233–2242.

D'Sa, E.J.; Hu, C.; Müller-Karger, F.E., and Carder, K.L., 2002. Estimation of colored dissolved organic matter and salinity fields in case 2 waters using SeaWiFS: examples from Florida Bay and Florida Shelf. *Journal of Earth System Sciences*, 111(3), 197–207.

D'Sa, E.J. and Ko, D.S., 2008. Short-term influences on suspended particulate matter distribution in the northern Gulf of Mexico: satellite and model observations. *Sensors*, 8(7), 4249–4264.

D'Sa, E.J. and Korobkin, M., 2008. Colored dissolved organic matter in the northern Gulf of Mexico using ocean color: seasonal trends in 2005. *Proceedings of SPIE*, 7105, 710505.

D'Sa, E.J. and Miller, R.L., 2003. Bio-optical properties in waters influenced by the Mississippi River during low flow conditions. *Remote Sensing of Environment*, 84(4), 538–549.

D'Sa, E.J.; Miller, R.L., and Del Castillo, C., 2006. Bio-optical properties and ocean color algorithms for coastal waters influenced by the Mississippi River during a cold front. *Applied Optics*, 45(28), 7410–7428.

Feng, Z., 2009. Hydrodynamic Response to Cold Fronts along the Louisiana Coast. Baton Rouge, Louisiana: Louisiana State University, Master's thesis, 128p.

Ferrari, G.M. and Dowell, M.D., 1998. CDOM absorption characteristics with relation to fluorescence and salinity in coastal areas of the southern Baltic Sea. *Estuarine Coastal and Shelf Science*, 47(1), 91–105.

Gardner, G.B.; Chen, R.F., and Berry, A., 2005. High-resolution meaurments of chromophoric dissolved organic matter (CDOM) fluorescence in the Neponset River Estuary, Boston Harbor, MA. *Marine Chemistry*, 96, 137–154.

Griffin, C.G.; Frey, K.E.; Rogan, J., and Holmes, R.M., 2011. Spatial and interannual variability of dissolved organic matter in the Kolyma River, East Siberia, observed using satellite imagery. *Journal of Geophysical Research*, 116(G3), 12p.

Hitchcock, G.L.; Chen, R.F.; Gardner, G.B., and Wiseman, W.J., 2004. A Lagrangian view of fluorescent chromophoric dissolved organic matter distributions in the Mississippi River plume. *Marine Chemistry*, 89, 225–239.

Jarosz, E., 1997. Summer flow regime on the Louisiana inner shelf. Baton Rouge, Louisiana: Louisiana State University, Master's thesis, 74p.

Jarosz, E. and Murray, S., 2005. Velocity and transport characteristics of the Louisiana-Texas coastal current. *Circulation in the Gulf of Mexico: Observations and Models Geophysical Monograph Series 161,* pp. 143–156.

Jolliff, J.K.; Walsh, J.J.; He, R.Y.; Weisberg, R.; Stovall-Leonard, A.; Coble, P.G.; Conmy, R.; Heil, C.; Nababan, B.; Zhang, H.Y.; Hu, C.M., and Müller-Karger, F.E., 2003. Dispersal of the Suwannee River plume over the West Florida shelf: simulation and observation of the optical and biochemical consequences of a flushing event. *Geophysical Research Letters*, 30(13), 1709.

Kahru, M. and Mitchell, B.G., 2001. Seasonal and nonseasonal variability of satellite-derived chlorophyll and colored dissolved

organic matter concentration in the California Current. *Journal of Geophysical Research*, 106, 2517–2529.
Ko, D.S.; Martin, P.J.; Rowley, C.D., and Preller, R.H., 2008. A real-time coastal ocean prediction experiment for MREA04. *Journal of Marine Systems*, 69(1–2), 17–28.
Kowalczuk, P., 1999. Seasonal variability of yellow substance absorption in the surface layer of the Baltic Sea. *Journal of Geophysical Research*, 104(C12), 30047–30058.
Le Fouest, V.; Zakardjian, B.; Saucier, F.J., and Cizmeli, S.A., 2006. Application of SeaWIFS- and AVHRR-derived data for mesoscale and regional validation of a 3-D high-resolution physical-biological model of the Gulf of St. Lawrence (Canada). *Journal of Marine Systems*, 60, 30–50.
Li, Y.; Nowlin Jr, W.D., and Reid, R.O., 1997. Mean hydrographic fields and their interannual variability over the Texas-Louisiana continental shelf in spring, summer and fall. *Journal of Geophysical Research*, 102(C1), 1027–1049.
Lohrenz, S.E.; Dagg, M.J., and Whitledge, T.E., 1990. Enhanced primary production at the plume oceanic interface of the Mississippi River. *Continental Shelf Research*, 10(7), 639–664.
Mannino, A.; Russ, M.E., and Hooker, S.B., 2008. Algorithm development and validation for satellite-derived distributions of DOC and CDOM in the US Middle Atlantic Bight. *Journal of Geophysical Research*, 113(C07051), 19p.
Martin, P.J., 2000. A description of the Navy Coastal Ocean Model Version 1.0. Stennis Space Center, Mississippi: Naval Research Laboratory, *NRL Report NRL/FR/7322–009962*, 39 p.
Martínez-López, B. and Zavala-Hidalgo, J., 2009. Seasonal and interannual variability of cross-shelf transports of chlorophyll in the Gulf of Mexico. *Journal of Marine Systems*, 77(1–2), 1–20.
Moran, M.A. and Zepp, R.G., 1997. Role of photoreactions in the formation of biologically labile compounds from dissolved organic matter. *Limnology and Oceanography*, 42(6), 1307–1316.
Müller-Karger, F.E.; Walsh, J.J.; Evans, R.H., and Meyers, M.B., 1991. On the seasonal phytoplankton concentration and sea surface temperature cycles of the Gulf of Mexico as determined by satellites, *Journal of Geophysical Research*, 96(C7), 12,645–12,665.
Murray, S.P.; Jarosz, E., and E.T. Weeks, III, 1998. Physical oceanographic observations of the coastal plume. *In*: Murray, S.P. (ed.), *An Observational Study of the Mississippi-Atchafalaya Coastal Plume*. New Orleans, Lousiana: Minerals Management Service, pp. 5–105.
Nelson, N.B.; Siegel, D.A.; Carlson C.A.; Swan, C.; Smethie, W.M., and Khatiwala, S., 2007. Hydrography of chromophoric dissolved organic matter in the North Atlantic. *Deep-Sea Research I*, 54, 710–731.
Nowlin, W.D.; Jochens, A.E.; Dimarco, S.F.; Reid, R.O., and Howard, M.K., 2005. Low-frequency circulation over the Texas-Louisiana shelf. *In:* Circulation in the Gulf of Mexico: observations and models. *Geophysical Monograph Series*, 161, 219–240.
Oey, L.Y., 1995. Eddy-forced and wind-forced shelf circulation. *Journal of Geophysical Research*, 100(C5), 8621–8637.
Opsahl, S. and Benner, R., 1998. Photochemical reactivity of dissolved lignin in river and ocean waters. *Limnology and Oceanography*, 43(6), 1297–1304.
Osburn, C.L. and Morris, D.P., 2003. Photochemistry of chromophoric dissolved organic matter in natural waters. *In*: Hebling, W.E. and Zagarese, H.E. (eds.), *UV Effects in Aquatic Organisms and Ecosystems*. Cambridge, U.K.: Royal Society of Chemistry, pp. 187–209.
Osburn, C.L.; O'Sullivan, D.W., and Boyd, T.J., 2009b. Increases in the longwave photobleaching of chromophoric dissolved organic matter in coastal waters. *Limnology and Oceanography*, 54, 145–159.
Osburn, C.L.; Retamal, L., and Vincent, W.F., 2009a. Photoreactivity of chromophoric dissolved organic matter transported by the Mackenzie River to the Beaufort Sea. *Marine Chemistry*, 115, 10–20.
Shulman, I.; Moline, M.A.; Penta, B.; Anderson, S.; Oliver, M., and Haddock, S.H.D., 2011. Observed and modeled bio-optical, bioluminescent, and physical properties during a coastal upwelling event in Monterey Bay, California. *Journal of Geophysical Research*, 116(C01018), 13p.
Stedmon, C.A. and Markager, S., 2003. Behaviour of the optical properties of coloured dissolved organic matter under conservative mixing. *Estuarine Coastal and Shelf Science*, 57(5–6), 973–979.
Stedmon, C.A.; Markager, S., and Kaas, H., 2000. Optical properties and signatures of chromophoric dissolved organic matter (CDOM) in Danish coastal waters. *Estuarine, Coastal and Shelf Science*, 51, 267–278.
Tehrani, N.C.; D'Sa, E.J.; Osburn, C.L.; Bianchi, T.S., and Schaeffer, B.A., 2013. Chromophoric dissolved organic matter and dissolved organic carbon from sea-viewing wide field-of-view sensor (SeaWiFS), moderate resolution imaging spectroradiometer (MODIS) and MERIS sensors: case study for the Northern Gulf of Mexico. *Remote Sensing*, 5, 1439–1464.
Toming, K.; Arst, H.; Paavel, B.; Laas, A., and Noges, T., 2009. Spatial and temporal variations in coloured dissolved organic matter in large and shallow Estonian waterbodies. *Boreal Environment Research*, 14, 959–970.
Uher, G.; Hughes, C.; Henry, G., and Upstill-Goddard, R.C., 2001. Non-conservative mixing behavior of colored dissolved organic matter in a humic-rich, turbid estuary. *Geophysical Research Letters*, 28(17), 3309–3312.
Vodacek, A.; Blough, N.V.; Degrandpre, M.D.; Peltzer, E.T., and Nelson, R.K., 1997. Seasonal variation of CDOM and DOC in the Middle Atlantic Bight: terrestrial inputs and photooxidation. *Limnology and Oceanography*, 42(4), 674–686.
Walker, N.D., 2005. Wind- and eddy-related shelf/slope circulation processes and coastal upwelling in the northwestern Gulf of Mexico. *In*: Sturges, W. and Lugo-Fernandez, A. (eds.), *New Developments in the Circulation of the Gulf of Mexico*. Washington, DC: American Geophysical Union Monograph, pp. 295–314.
Walker, N.D.; Fargion, G.; Rouse, L., and Biggs, D., 1994. The Great Flood of summer 1993: Mississippi River discharge studied. *EOS, Transactions, American Geophysical Union*, 75(36), 409–415.
Walker, N.D. and Hammack, A.B., 2000. Impacts of winter storms on circulation and sediment transport: Atchafalaya-Vermilion Bay Region, Louisiana, U.S.A. *Journal of Coastal Research*, 16(4), 996–1010.
Walker, N.D.; Huh, O.K.; Rouse Jr., L.J., and Murray, S.P., 1996. Evolution and structure of a coastal squirt off the Mississippi River delta: Northern Gulf of Mexico, *Journal of Geophysical Research*, 101(C9), 20,643–20,655.
Walker, N.D. and Rabalais, N.N., 2006. Relationships among satellite chlorophyll a, river inputs, and hypoxia on the Louisiana continental shelf, Gulf of Mexico. *Estuaries and Coasts*, 29(6B), 1081–1093.
Walker, N.D.; Wiseman, W.J.; Rouse, L.J., and Babin, A., 2005. Effects of river discharge, wind stress, and slope eddies on circulation and the satellite-observed structure of the Mississippi River plume. *Journal of Coastal Research*, 21(6), 1228–1244.
Wiseman, W.J. and Kelly, F.J., 1994. Salinity variability within the Louisiana coastal current during the 1982 flood season. *Estuaries*, 17(4), 732–739.
Wiseman, W.J.; Rabalais, N.N.; Turner, R.E.; Dinnel, S.P., and MacNaughton, A., 1997. Seasonal and interannual variability within the Louisiana coastal current: stratification and hypoxia. *Journal of Marine Systems*, 12, 237–248.
Yoder, J.A., 1999. Considerations for Complementary Missions. Dartmouth, Canada, Report *the International Ocean Colour Coordinating Group (IOCCG) No. 2*.